MODIS DATA STUDY

TEAM PRESENTATION

June 15, 1990

AGENDA

1. MODIS Earth Location Computation Requirements Document Template (Ardanuy, Team)

2. A Preliminary Investigation of Possible Tilt Strategies for MODIS-T (Gregg)

MODIS EARTH LOCATION COMPUTATION REQUIREMENTS

D. Han and H. L. Kyle
NASA/Goddard Space Flight Center
Greenbelt, MD

P. Ardanuy, W. Gregg, D. Hoyt, A. McKay, and G. Riggs
Research and Data Systems Corporation
Greenbelt, MD

M. Andrews and J. Schols
General Sciences Corporation
Laurel, MD

July 1990

MODIS NAVIGATION REQUIREMENTS

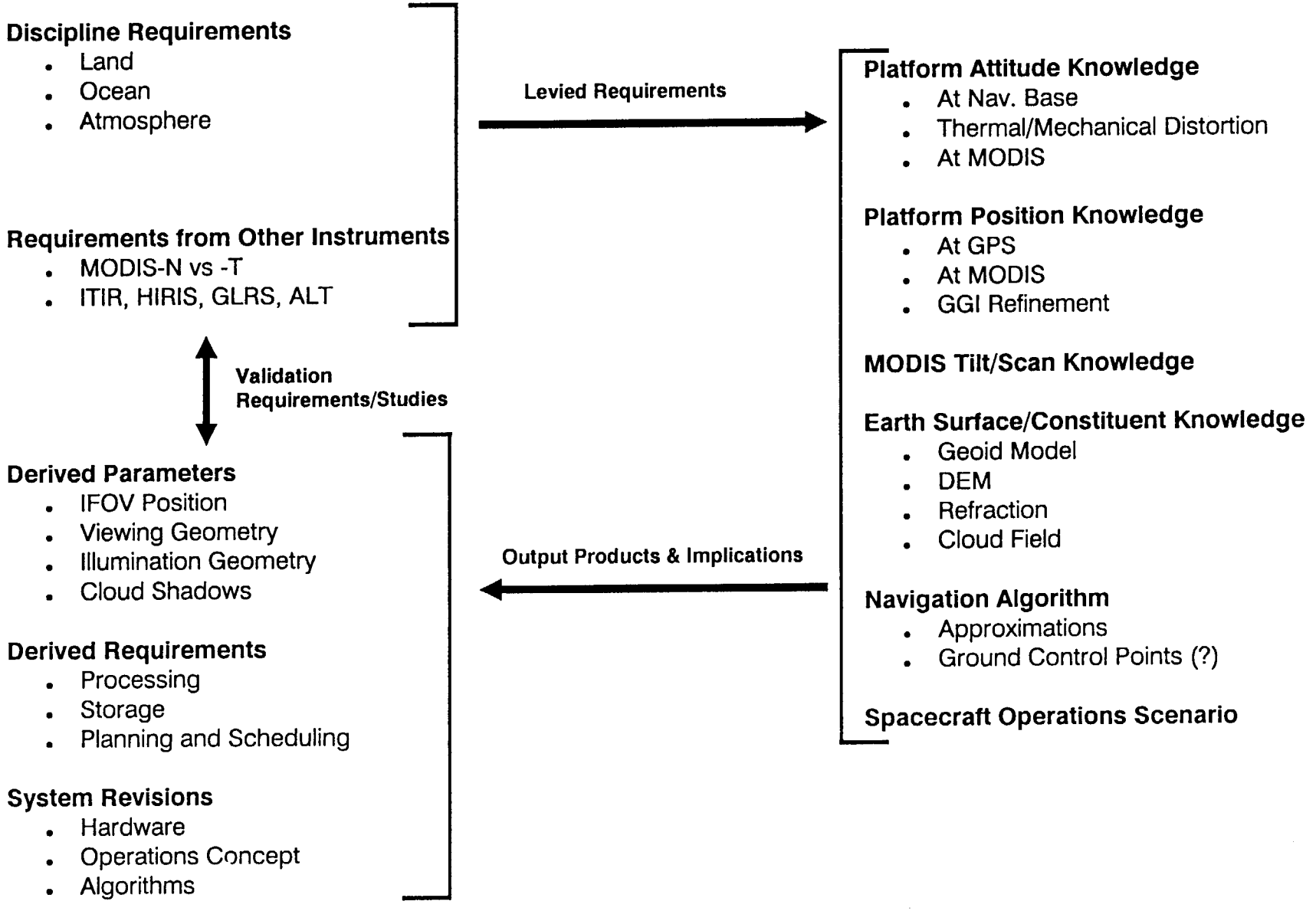

Table of Contents

1 INTRODUCTION (Ardanuy)

TEXT WILL BE INSERTED HERE.

Issue:

THIS SPACE WILL BE FOR STATING THE ISSUE

2 SCIENCE REQUIREMENTS

TEXT WILL BE INSERTED HERE.

Issue:

THIS SPACE WILL BE FOR STATING THE ISSUE

2.1 Discipline Requirements

TEXT WILL BE INSERTED HERE.

Issue:

THIS SPACE WILL BE FOR STATING THE ISSUE

2.1.1 Land (Riggs, Schols)

TEXT WILL BE INSERTED HERE.

Issue:

THIS SPACE WILL BE FOR STATING THE ISSUE

2.1.2 Ocean (Gregg)

TEXT WILL BE INSERTED HERE.

Issue:

THIS SPACE WILL BE FOR STATING THE ISSUE

2.1.3 Atmosphere (Andrews, Hoyt)

TEXT WILL BE INSERTED HERE.

Issue:

THIS SPACE WILL BE FOR STATING THE ISSUE

2.2 Other Instrument Requirements (TBD)

TEXT WILL BE INSERTED HERE.

Issue:

THIS SPACE WILL BE FOR STATING THE ISSUE

3 INPUT DATA REQUIREMENTS

TEXT WILL BE INSERTED HERE.

Issue:

THIS SPACE WILL BE FOR STATING THE ISSUE

3.1 Platform Attitude Knowledge (Ardanuy, Schols)

TEXT WILL BE INSERTED HERE.

Issue:

THIS SPACE WILL BE FOR STATING THE ISSUE

3.1.1 At Nav. Base

TEXT WILL BE INSERTED HERE.

Issue:

THIS SPACE WILL BE FOR STATING THE ISSUE

3.1.2 Thermal and Mechanical Distortion

TEXT WILL BE INSERTED HERE.

Issue:

THIS SPACE WILL BE FOR STATING THE ISSUE

3.1.3 At MODIS

TEXT WILL BE INSERTED HERE.

Issue:

THIS SPACE WILL BE FOR STATING THE ISSUE

3.2 Platform Position Knowledge (Ardanuy, Schols)

TEXT WILL BE INSERTED HERE.

Issue:

THIS SPACE WILL BE FOR STATING THE ISSUE

3.2.1 GPS

TEXT WILL BE INSERTED HERE.

Issue:

THIS SPACE WILL BE FOR STATING THE ISSUE

3.2.2 At MODIS

TEXT WILL BE INSERTED HERE.

Issue:

THIS SPACE WILL BE FOR STATING THE ISSUE

3.2.3 GGI Refinements

TEXT WILL BE INSERTED HERE.

Issue:

THIS SPACE WILL BE FOR STATING THE ISSUE

3.3 MODIS Instrument Knowledge (Gregg)

TEXT WILL BE INSERTED HERE.

Issue:

THIS SPACE WILL BE FOR STATING THE ISSUE

3.4 Spacecraft Operations Scenario (McKay)

TEXT WILL BE INSERTED HERE.

Issue:

THIS SPACE WILL BE FOR STATING THE ISSUE

3.5 Ancillary Data

TEXT WILL BE INSERTED HERE.

Issue:

THIS SPACE WILL BE FOR STATING THE ISSUE

4 MODELS AND ALGORITHMS

TEXT WILL BE INSERTED HERE.

Issue:

THIS SPACE WILL BE FOR STATING THE ISSUE

4.1 Earth Knowledge

TEXT WILL BE INSERTED HERE.

Issue:

THIS SPACE WILL BE FOR STATING THE ISSUE

4.1.1 Geoid Model (McKay)

TEXT WILL BE INSERTED HERE.

Issue:

THIS SPACE WILL BE FOR STATING THE ISSUE

4.1.2 Digital Elevation Model (Riggs, etc.)

TEXT WILL BE INSERTED HERE.

Issue:

THIS SPACE WILL BE FOR STATING THE ISSUE

4.1.3 Refraction (Hoyt)

TEXT WILL BE INSERTED HERE.

Issue:

THIS SPACE WILL BE FOR STATING THE ISSUE

4.1.4 Cloud Field (Barker)

TEXT WILL BE INSERTED HERE.

Issue:

THIS SPACE WILL BE FOR STATING THE ISSUE

4.2 Navigation Algorithm

TEXT WILL BE INSERTED HERE.

Issue:

THIS SPACE WILL BE FOR STATING THE ISSUE

4.2.1 Approximations (Watson, Schols)

TEXT WILL BE INSERTED HERE.

Issue:

THIS SPACE WILL BE FOR STATING THE ISSUE

4.2.2 Ground Control Points (Andrews, Riggs)

TEXT WILL BE INSERTED HERE.

Issue:

THIS SPACE WILL BE FOR STATING THE ISSUE

5 OUTPUT PRODUCTS, DERIVED SYSTEMS REQUIREMENTS, AND IMPLICATIONS

TEXT WILL BE INSERTED HERE.

Issue:

THIS SPACE WILL BE FOR STATING THE ISSUE

5.1 Derived Parameters

TEXT WILL BE INSERTED HERE.

Issue:

THIS SPACE WILL BE FOR STATING THE ISSUE

5.1.1 IFOV Position (Ardanuy, Andrews)

TEXT WILL BE INSERTED HERE.

Issue:

THIS SPACE WILL BE FOR STATING THE ISSUE

5.1.2 Viewing Geometry (Ardanuy, Andrews)

TEXT WILL BE INSERTED HERE.

Issue:

THIS SPACE WILL BE FOR STATING THE ISSUE

5.1.3 Illumination Geometry (Ardanuy, Andrews)

TEXT WILL BE INSERTED HERE.

Issue:

THIS SPACE WILL BE FOR STATING THE ISSUE

5.1.4 Cloud Shadows (Barker)

TEXT WILL BE INSERTED HERE.

Issue:

THIS SPACE WILL BE FOR STATING THE ISSUE

5.2 Derived Requirements

TEXT WILL BE INSERTED HERE.

Issue:

THIS SPACE WILL BE FOR STATING THE ISSUE

5.2.1 Processing (Ardanuy)

TEXT WILL BE INSERTED HERE.

Issue:

THIS SPACE WILL BE FOR STATING THE ISSUE

5.2.2 Storage (Centralized and Distributed) (Ardanuy, etc.)

TEXT WILL BE INSERTED HERE.

Issue:

THIS SPACE WILL BE FOR STATING THE ISSUE

5.2.3 Processing and Storage Trade Studies (McKay, Andrews)

TEXT WILL BE INSERTED HERE.

Issue:

THIS SPACE WILL BE FOR STATING THE ISSUE

5.2.4 Planning and Scheduling (McKay)

TEXT WILL BE INSERTED HERE.

Issue:

THIS SPACE WILL BE FOR STATING THE ISSUE

A Preliminary Investigation of

Possible Tilt Strategies for MODIS-T

Introduction

The purpose of this report is to examine the sun glitter distributions observed by the Moderate Resolution Imaging Spectrometers (MODIS), specifically MODIS-T, in an effort to make preliminary observations of potential tilting strategies. As such, we are now able to draw the MODIS Science Team's attention to a number of important issues which must be further studied before optimal MODIS operational concepts, including tilt strategies, may be determined and implemented.

Specular reflection of solar irradiance from the ocean surface, or sun glint (glitter), can contribute more than 1000 times the radiance emanating from beneath the surface to the total radiance received by a spaceborne platform for typical chlorophyll concentrations. Thus mechanisms to avoid this sun glint and remove it are essential for remote sensing of ocean color. The ability of a sensor to tilt fore and aft the sub-satellite track is a successful mechanism for minimizing this radiance contribution. MODIS-T, which is proposed to fly on the Earth Observing System (Eos) in 1997/8, has a tilt capability of $\pm 50^{\circ}$.

Although MODIS-T is not scheduled for launch for several years, these analyses are important and timely for two reasons. First, although the sensor was originally designed primarily to facilitate ocean remote sensing, it now is proposed to operate in so-called composite mode. In this mode, the signal-to-noise ratio (SNR) changes automatically within a scan to be useful for land or ocean viewing. The tilt capability of MODIS-T may be useful for investigations of the bi-directional reflectance function (BRDF) over land regions. Wherever MODIS-T does not require tilt for ocean viewing, its non-tilting companion sensor, MODIS-N, may be used for ocean observations, freeing up MODIS-T for BRDF investigations. Thus it is important to know where MODIS-T does not require tilt for sun glint avoidance so that it may be used in planning scenarios for BRDF investigations.

Second, the MODIS-T tilt capability of $\pm 50^{\circ}$ is greater than the CZCS capability of $\pm 20^{\circ}$. It is not known whether higher tilts than 20° can be used to further minimize sun glint.

Thus we focus here on two issues: when can MODIS-T utilize zero tilt and still avoid sun glint, in order that the sensor be available for BRDF investigations, and will tilts greater than 20° be useful for sun glint avoidance?

In the investigations that follow, it is important to keep in mind

that sun glint avoidance is not the only issue in determining a tilt strategy. If it were, one would simply tilt at maximum throughout the orbit. Tilting, however, has two significant drawbacks: 1) it increases the path length that light must travel through the atmosphere, thereby reducing the relative contribution of water-leaving radiance to the total radiance received by the sensor and rendering ocean observations less accurate, and 2) changes in tilt from aft to fore, as required for sun glint avoidance at the latitude of solar declination, results in a loss of Earth coverage, even for instantaneous tilt changes. Fore to aft tilts do not result in loss of coverage. Assessment of a tilt strategy, therefore, must consider these two issues in addition to sun glint avoidance.

Background

Physics of Sun Glint

Sun glint results from specular reflection of solar irradiance by the sea surface, as noted in the introduction. For a flat ocean (one for the there is no wind and the ocean surface is mirror-like), the maximum sun glint occurs where the solar zenith angle (θ_o) and spacecraft zenith angle (θ) of a point on the surface are equal, and where the relative azimuth ($\phi-\phi_o$, where ϕ is the spacecraft azimuth angle of a vector from the point to the sub-satellite ground point measured from true north and ϕ_o is the solar azimuth angle, defined similarly except with respect to the sub-solar point) is 180°.

The situation is considerably complicated by wind, however, as described by Cox and Munk (1954). Wind roughens the sea surface, producing a reduced intensity of sun glint under no wind, but spreading out the pattern of glint over the ocean surface.

These effects are described by Cox and Munk (1954) and Viollier et al. (1981) by

$$L_g(\theta,\phi,\theta_o,\phi_o,V,\lambda) = F_o(\lambda)\rho p(\theta,\phi,\theta_o,\phi_o,V)/(4\cos\theta\cos^4\theta_o) \qquad (1)$$

$p(\theta,\phi,\theta_o,\phi_o,V)$ is the probability of seeing sun glitter in the direction θ,ϕ given the sun in position θ_o,ϕ_o as a function of wind speed. $F_o(\lambda)$ is the extraterrestrial solar irradiance corrected for Earth-Sun distance.

If $L_g(\lambda)$ is the sun glint radiance at the surface, $tL_g(\lambda)$ is that received by the sensor, where t is the diffuse transmittance from the Earth to the satellite

$$t = \exp[-(\tau_r/2 + \tau_{oz})/\cos\theta] \qquad (2)$$

where τ_r is the Rayleigh optical thickness, τ_{oz} is the ozone optical

thickness.

For CZCS processing, a 6 m s^{-1} global mean wind speed was assumed. In the following simulations, we also assume a mean wind speed of 6 m s^{-1}.

It should be noted that At a mean wind speed of 6 m s^{-1}, the Cox and Munk theory contains an inherent error of $\pm$ 0.8 m s^{-1}. This is due to the neglect of wind direction and atmospheric stability (P. Ardanuy, personal communication), among other variables, in the Cox and Munk relation. Thus, a threshold of 0.8 m s^{-1} accuracy stands as the ultimate accuracy level required by MODIS, unless simultaneous improvements are made in the relation between sea surface roughness and sun glitter.

Simulation Method

MODIS (Eos) Orbital Simulation/Earth Location

Orbital simulation and Earth location, including solar and viewing geometries, were computed using the CZCS Geolocation Algorithm Report (Wilson et al., 1981) into which Eos orbital parameters and MODIS-T instrument characteristics were substituted (Table 1). The code was modified to correct the computation of spacecraft azimuth angle and several quadrant ambiguities in computation of azimuth, longitude, and latitude. Most of these corrections were important only near the poles and the dateline.

Table 1. EOS orbital simulation parameters and MODIS-T instrument characteristics.

EOS Orbital Parameters

Altitude	705	km
Orbital Repeat Time	16	days (233 orbits)
Period	98.9	minutes
Inclination	98.25	degrees
Equatorial Crossing Time	1:30	local time

MODIS-T Instrument Characteristics

Scan Width	$\pm$ 45°
IFOV	1.56 mrad (0.089°)
Ground IFOV at nadir	1.1 km
Pixels Along Scan	1007
Ground Coverage Along Scan	1500 km (at nadir; no tilt)
Tilt	$\pm$ 50°
Pixels Along Track	30

Ground Coverage Along Track	32.6 km (at nadir; no tilt)
Successive Orbit Equatorial Crossing Longitude	-24.721°

MODIS Radiance Simulation

In order to understand the consequences of sun glint, we required knowledge of its relative contribution to the radiance emanating from the ocean. This knowledge was obtained by simulating the optical properties of the water under different concentrations of chlorophyll.

These optical properties were simulated using the model of Sathyendranath and Platt (1988). Five chlorophyll concentrations were used: 0.05, 0.5, 1.0, 5.0, and 10.0 mg m^{-3}, These optical properties produced a spectral set of normalized water-leaving radiances for MODIS-T bands according to the model of Gordon et al. (1988). Normalized water-leaving radiances $[L_w]_N$ are related to water-leaving radiances by

$$L_w = [L_w]_N \cos\theta_o \, t_o \qquad (3)$$

(λ-dependence has been suppressed) where

$$t_o = \exp[-(\tau_r/2 + \tau_{oz})/\cos\theta_o] \qquad (4)$$

or the transmittance of the atmosphere to solar irradiance, neglecting aerosols. Normalized water-leaving radiances are thus the water-leaving radiance expected for a sun at nadir and with atmosphere removed.

Rayleigh radiance, used here for assessing atmospheric influences on tilt strategies, was computed using a single scattering approximation (Gordon et al., 1983). Mean extraterrestrial irradiance was taken from Neckel and Labs (1984) as the mean over the MODIS-T bands, and ozone absorption coefficients were taken from Bird and Riordan (1986). The radiance contribution from the ocean is that leaving the water multiplied by the atmospheric transmittance from the surface to the satellite, tL_w, where t is as defined in Eqn. 2.

Simulation Results

The simulated distribution of sun glint as viewed by an untilted MODIS-T at the equinox for 0 wind speed is shown in Figure 1. In this and subsequent figures, latitude is depicted on the ordinate and the cross-track scan on the abscissa. Units are radiance units, mW cm^{-2} μm^{-1} sr^{-1}, and are shown for tL_g at 500 nm, because

previous analyses had shown the glint radiance to be highest at this wavelength.

The zero wind, zero tilt case produces a small, intense pattern of sun glint, with values exceeding 100 mW cm^{-2} μm^{-1} sr^{-1} at maximum. These values exceed the saturation radiance of MODIS-T.

At a 6 m s^{-1} wind speed, the glint pattern is spread out but diminished in magnitude (Figure 2). Maximum values are now about 11 mW cm^{-2} μm^{-1} sr^{-1}, less than the saturation radiance but still twice as high as the expected Rayleigh radiance.

Substantial reduction in the intensity and distribution of sun glint is achieved by tilting the sensor +10° northward of the solar declination latitude and -20° southward (Figure 3). The 0.5 mW cm^{-2} μm^{-1} sr^{-1} contour is now located at 30° N latitude as opposed to near 45° N for the no-tilt case. Some evidence of loss of Earth coverage is apparent. Figures 2 and 3 illustrate the importance of sun glint avoidance procedures.

Figures 4 and 5 depict the continuing reduction in sun glint intensity and distribution with 20° and 30° tilts, such that maxima are ≈3 and ≈0.6 mW cm^{-2} μm^{-1} sr^{-1}, respectively. These figures illustrate the usefulness of higher tilts in minimizing sun glint, but also show the increased loss of Earth coverage near the solar declination latitude as a function of tilting from aft to fore.

Issue 1: When Can MODIS Utilize Zero Tilt?

In Figure 2 it was shown that sun glint radiances < 0.5 mW cm^{-2} μm^{-1} sr^{-1} were obtained north of 45° N latitude at a wind speed of 6 m s^{-1} even with no tilt. However, the sun glint radiance received by the sensor is not the entire picture.

If the sun glint radiance is known, then it may be subtracted from the radiance received by the sensor to obtain the water-leaving radiance. In practice, however, it is not known but rather is computed by the wind speed, knowledge of which contains an uncertainty. Possible sources and errors of wind speed data in the MODIS era are shown in Table 2.

Table 2. Sources and accuracies of wind speed data.

Source	Accuracy
NMC	± 5 m s^{-1}
SCANSCAT	± 1-2 m s^{-1}
LAWS	± 1 m s^{-1}

We must therefore consider the error in sun glint due to wind speed knowledge uncertainty in our assessment of when to use zero tilt. Furthermore, the sun glint radiance must be compared to the radiance emanating from beneath the surface and into the sensor, or tL_w, the diffusely transmitted water-leaving radiance, in order to gain perspective into its importance.

In Figure 6 the distribution of $tL_w(440)$ is shown for a 10° tilt. $tL_w(440)$ was chosen because it is a wavelength involved in the pigment algorithms for the CZCS (Gordon, et al., 1983). Radiance resulting from a chlorophyll concentration of 1 mg m^{-3} is shown. At higher chlorophyll concentrations the water-leaving radiance at 440 nm is no longer used (Gordon, 1988) because nearly all of the light at this wavelength is absorbed by phytoplankton. As shown in Figure 6, tL_w changes as a function of latitude, which is due to reduction by an increased atmospheric path length.

If we assume that wind speeds will be known to within 5 m s^{-1}, the result will be that we will under- or overestimate sun glint radiance by a maximum of that due to a 5 m s^{-1} error in wind speed. If we assume that 6 m s^{-1} is a global mean, as for CZCS processing, then the wind speed may be 11 or 1 m s^{-1} and remain within our knowledge.

This error in wind speed will produce greater or less sun glint radiance than we have predicted using a mean wind speed. If the atmospheric correction algorithm for MODIS is conservative, as was the case for the CZCS, this "extra" or reduced sun glint radiance will produce an error in our estimated water-leaving radiance. To understand the significance of this radiance, we computed the ratio $\Delta tL_g(440)$ at 11 m s^{-1} and 6 m s^{-1} to $tL_w(440)$. Further, we used this ratio to indicate when it will be important to tilt to reduce sun glint radiance. We will let the ratio = 1 as the level at which sun glint radiance should be minimized. At this ratio, "extra" sun glint radiance from that obtained at wind speed of 6 m s^{-1} may produce double the actual tL_w, and reduced radiance may result in tL_w estimates of 0.

It must be pointed out that this analysis does not incorporate an atmospheric correction algorithm. In the CZCS atmospheric correction algorithm, non-predicted sun glint radiance was absorbed into the aerosol radiance term. This resulted in its implicit removal when the aerosol optical properties were such that their spectral effects were similar to those of sun glint (i.e., approximately spectrally neutral). For typical marine aerosols, this is not an unusual occurrence. In cases where the aerosol spectral optical behavior was different from that of sun glint, an error in aerosol radiance was generated, which propagated into the estimate of water-leaving radiance. In the analysis here, these effects are not incorporated since the MODIS atmospheric correction algorithm is not yet publicly available, and must be viewed as a preliminary analysis.

A plot of the ratio $\Delta tL_g(440)$ to $tL_w(440)$ is shown in Figure 7 for an untilted MODIS-T. Ratios greater than one extend all the way from -75° S to 75° N latitude. The unusual pattern of the ratio derives from the difference in glitter radiance at the wind speeds used. A 10° tilt reduces the ratio considerably, and we now see ratios < 1 northward of 50° N and southward of -45° S (Figure 8).

Before we conclude that a 10° tilt may be necessary for nearly the full ascending node for MODIS-T, we must investigate the effects of a 10° tilt on atmospheric path length. For this analysis we show the spacecraft zenith angles produced at the scan edges for various tilts (Figure 9) and the single-scattering Rayleigh radiance (at 440 nm) obtained at the scan edge for these tilts (Figure 10). These figures show that the increase in maximum spacecraft zenith angle and Rayleigh radiance are small for a 10° tilt, even at high latitudes.

We may then conclude that a 10° tilt may be necessary for MODIS-T from -75° S to 75° N for sun glint avoidance given 5 m s^{-1} wind speed uncertainty. Furthermore, a 10° tilt produces a small change in atmospheric path length and is an acceptable tilt strategy at high latitudes.

If wind speeds are known to 2 m s^{-1}, as may be obtained from active microwave scatterometers (see Table 2), then the requirement for tilt at high latitudes may be relaxed (Figure 11). With this error in wind speed, the ratio of $tL_g(440)$ to $tL_w(440)$ is less than 1 northward of 60° N and southward of -55° S. With greater knowledge of wind speeds, the requirement for tilt may be relaxed.

Issue 2: Are Higher Tilts than 20° Preferable?

Recall from Figures 3 and 4 that increasing the tilt from $\pm$20° to $\pm$30° produced nearly a five-fold decrease in sun glint intensity. Clearly such a reduction is advantageous, but we must first consider the implications on atmospheric path length and Earth coverage loss.

Referring to Figure 9, it was shown that an increase in tilt produced an exponential increase in maximum spacecraft zenith angle. The change in θ from 0 to 10° tilt was < 1°, but the change from 20° to 30° produced a change in of > 4° in θ. At a tilt of 50°, θ was 81°, while at 40° the spacecraft zenith angle was nearly 70°.

Considering the Rayleigh radiance at the scan edge for the various tilts (Figure 10) one gains more insight into the implications of various tilts. At a tilt of 40°, the Rayleigh radiance is double that at no tilt, and at a tilt of 50° is more than 5 times that at no tilt.

Higher tilts also produce a greater loss of Earth coverage as the tilt changes from aft to fore at the latitude of solar declination. These effect for tilts of 0 to 50° are listed in Table 3.

Tilts greater than 30° clearly produce high spacecraft zenith angles, high Rayleigh radiance and large Earth coverage loss. We may conclude that tilts greater than 30° are unacceptable for ocean remote sensing.

However, the situation is not so clear for 30° tilts. While there is less coverage, more Rayleigh radiance, and a greater maximum spacecraft zenith angle at 30° than at 20°, the atmospheric effects may be alleviated by better atmospheric correction for MODIS than for the CZCS, and the Earth coverage loss may be partially alleviated by MODIS-N.

Table 3. Coverage loss at Equator as a function of changing from aft to fore tilt. Assuming instantaneous tilt change.

Tilt	Coverage Loss
0°	0
10°	2.2° (244 km)
20°	4.6° (506 km)
30°	7.4° (813 km)
40°	11.0° (1209 km)
50°	16.4° (1807 km)

Coverage losses are < 1000 km for tilts < 40°.

Considering the loss of coverage from 20° to 30° tilt, the increase in Rayleigh radiance, and the reduction in sun glint radiance, one may conclude that a 30° tilt may be an improvement very near the latitude of solar declination. The loss of coverage is less important, although substantial, if MODIS-N is used to fill in areas missed by MODIS-T. This is a reasonable strategy despite the fact that MODIS-N does not tilt since Eos is in a 1:30 PM Equatorial Crossing Time orbit, and the right (east) half of a non-tilting sensor will still obtain useable water-leaving radiances (see Figure 2).

Discussion and Conclusions

The preliminary investigation here of possible tilt strategies for

MODIS-T is intended to yield some insights into the sensor's capabilities and deficiencies, and to aid the MODIS Science Team in planning and scheduling. The results are only preliminary because they do not contain a detailed assessment of the effects of sun glitter on atmospheric correction and the retrieval of water-leaving radiances. Thus the results presented here can be considered tentative, and must be used with caution.

The results do suggest that tilt strategies for MODIS-T have important implications for the land and ocean disciplines. The results suggest that MODIS-T may require a 10° tilt even at high latitudes if wind speed knowledge is only to $\pm$ 5 m s^{-1}, as is present knowledge. This result precludes the use of MODIS-T for BRDF investigations over land except over scans that are entirely over land, if ocean remote sensing is considered a priority with MODIS-T. If wind speed is known to higher accuracy, these tilt requirements at high latitudes may be relaxed.

The results also suggest that increasing the tilt from 20°, as used with the CZCS, to 30° near the solar declination may be advantageous in reducing sun glitter contamination, only if MODIS-N is available for ocean remote sensing to partially fill in areas of lost Earth coverage and only if sufficiently accurate atmospheric correction methods are available to reduce atmospheric contributions. Otherwise, the increase of coverage loss of 300 km in this biologically active region may be unacceptable for global observations of ocean color.

Finally, more complete analyses using the MODIS atmospheric correction algorithm are required at this point to refine the issues of tilt strategy. It is our hope that this report will provide a starting point for such analyses, and will allow formulation of the tilt possibilities for preliminary planning and scheduling operational purposes until such studies are completed.

References

Bird, R.E. and C. Riordan, 1986. Simple solar spectral model for direct and diffuse irradiance on horizontal and tilted planes at the Earth's surface for cloudless atmospheres. Journal of Climate and Applied Meteorology 25: 87-97.

Cox, C. and W. Munk, 1954. Measurement of the roughness of the sea surface from photographs of the sun's glitter. J. Mar. Res. 44: 838-850.

Gordon, H.R., 1988. Ocean color remote sensing systems: radiometric requirements. Recent advances in sensors, radiometry, and data processing for remote sensing, Proceeding of the SPIE, P.N. Slater, ed., pp. 151-165.

Gordon, H.R., D.K. Clark, J.W. Brown, O.B. Brown, R.H. Evans, and W.W. Broenkow, 1983. Phytoplankton pigment concentrations in the Middle Atlantic Bight: comparison of ship determinations and CZCS estimates. Applied Optics 22: 20-36.

Gordon, H.R. and D.J. Castano, 1987. Coastal Zone Color Scanner atmospheric correction algorithm: multiple scattering effect. Applied Optics 26: 2111-2122.

Gordon, H.R., O.B. Brown, R.H. Evans, J.W. Brown, R.C. Smith, K.S. Baker, and D.K. Clark, 1988. A semianalytic radiance model of ocean color. Journal of Geophysical Research 93: 10909-10924.

Neckel, H. and D. Labs, 1984. The solar radiation between 3300 and 12500 A. Solar Physics 90: 205-258.

Sathyendranath, S. and T. Platt, 1988. The spectral irradiance field at the surface and in the interior of the ocean: a model for applications in oceanography and remote sensing. Journal of Geophysical Research 93: 9270-9280.

Viollier, M., D. Tanre, and P.Y. Deschamps, 1980. An algorithm for remote sensing of water color from space. Boundary-Layer Meteorology 18: 247-267.

Wilson, W.H., R.C. Smith, and J.W. Nolten, 1981. The CZCS geolocation algorithms. SIO Ref. 81-32, Scripps Institution of

Oceanography, La Jolla, CA. 37 pp.

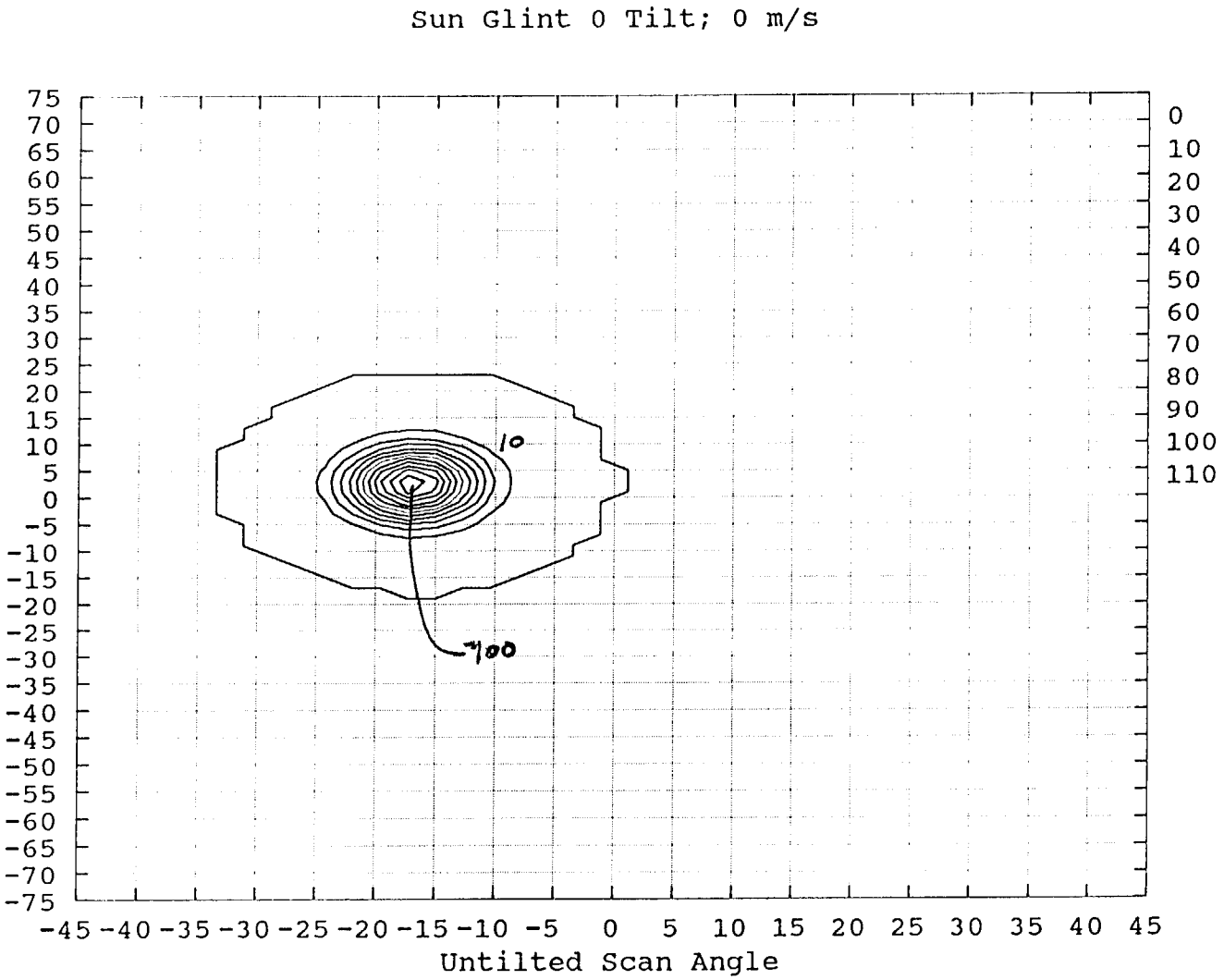

Figure 1. Sun glint radiance distribution obtained by MODIS-T for 0 tilt, with a 0 m s^{-1} wind speed. Latitude of the pixel is on the ordinate, untilted scan angle on the abscissa. Units are mW cm^{-2} μm^{-1} sr^{-1}. The numbers on the right-hand side denote the major contour levels (in bold).

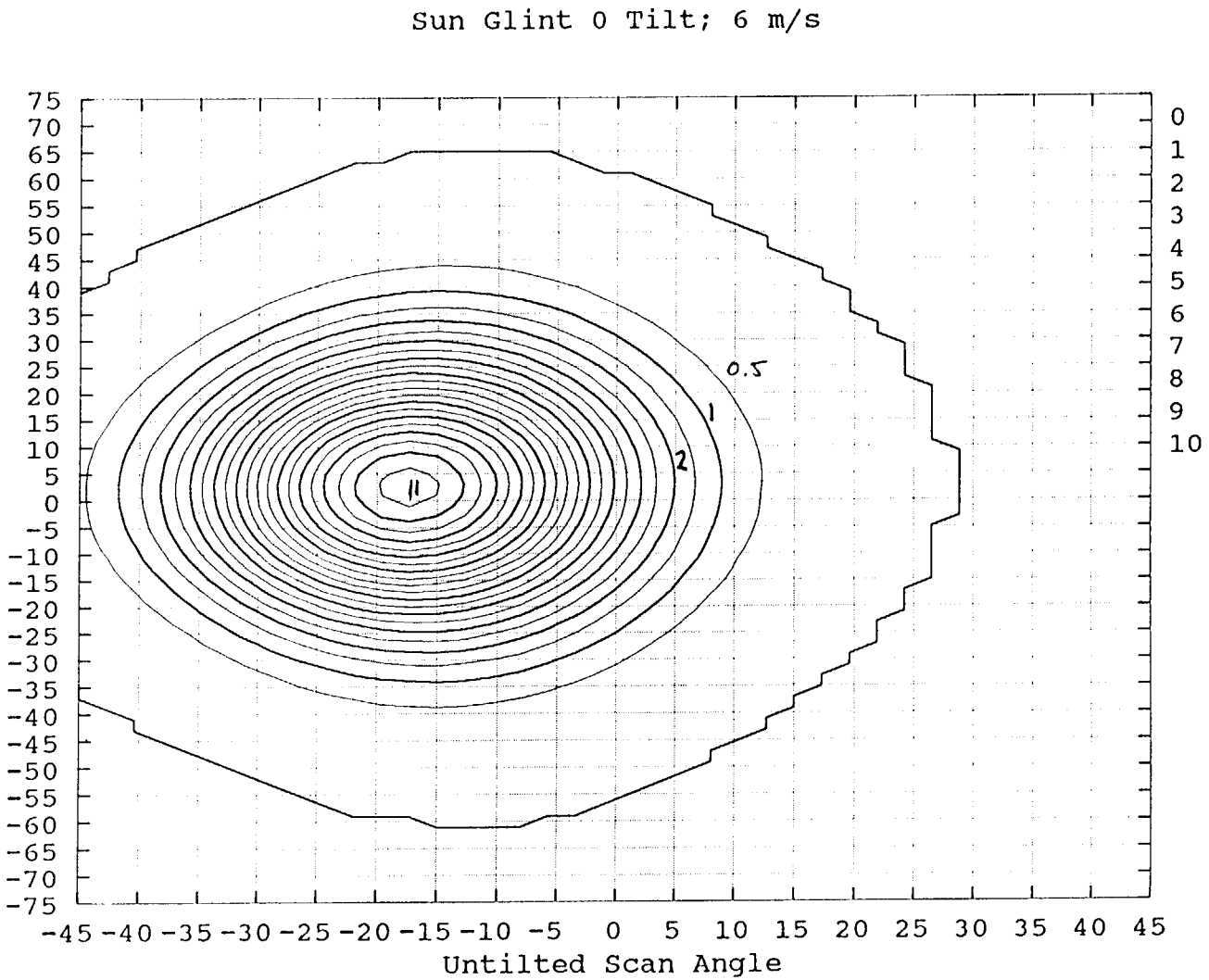

Figure 2. Sun glint radiance distribution obtained by MODIS-T for 0 tilt, with a 6 m s^{-1} wind speed. Latitude of the pixel is on the ordinate, untilted scan angle on the abscissa. Units are mW cm^{-2} μm^{-1} sr^{-1}. The numbers on the right-hand side denote the major contour levels (in bold).

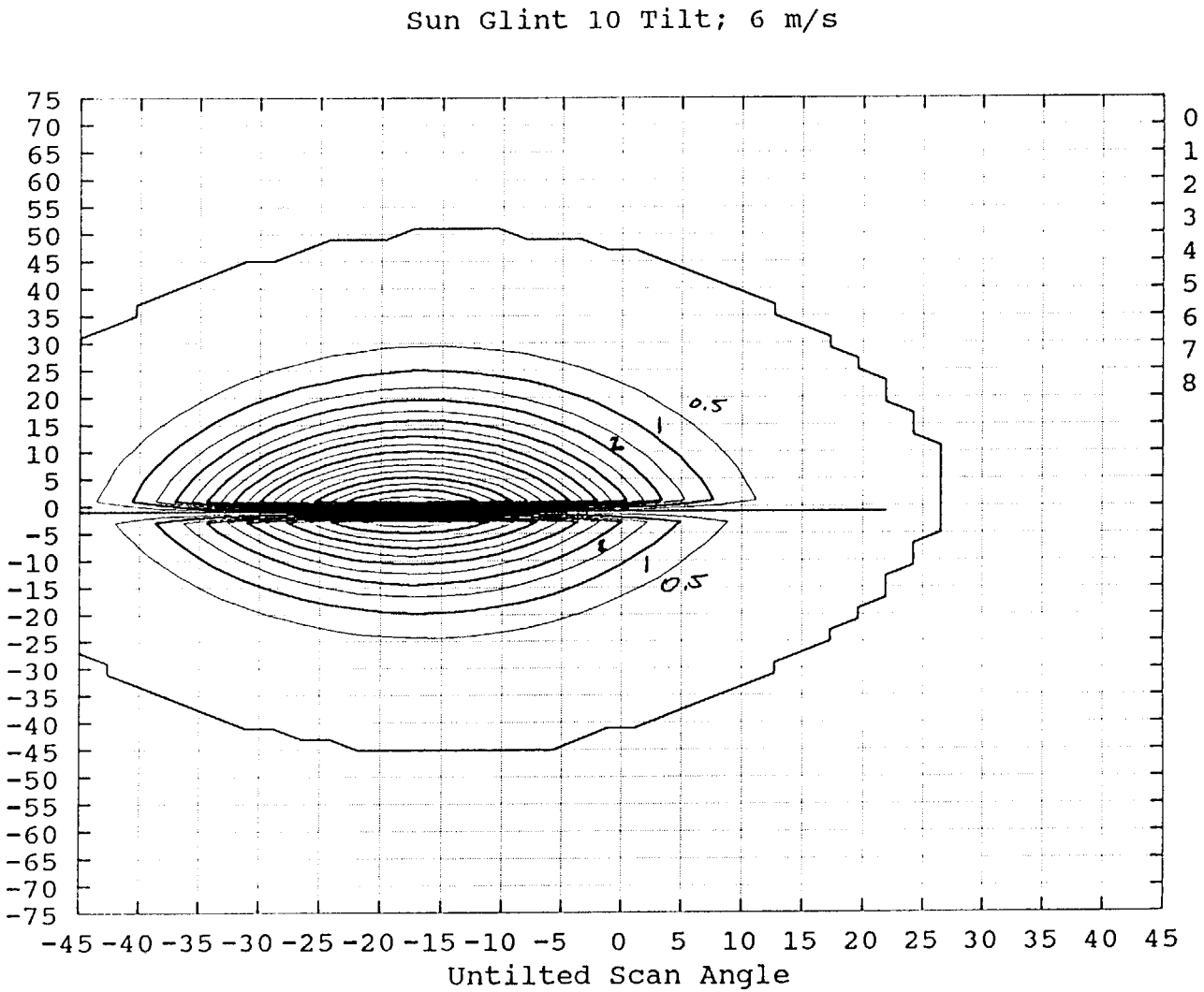

Figure 3. Sun glint radiance distribution obtained by MODIS-T for 10° tilt, with a 6 m s^{-1} wind speed. Latitude of the pixel is on the ordinate, untilted scan angle on the abscissa. Units are mW cm^{-2} μm^{-1} sr^{-1}. The numbers on the right-hand side denote the major contour levels (in bold).

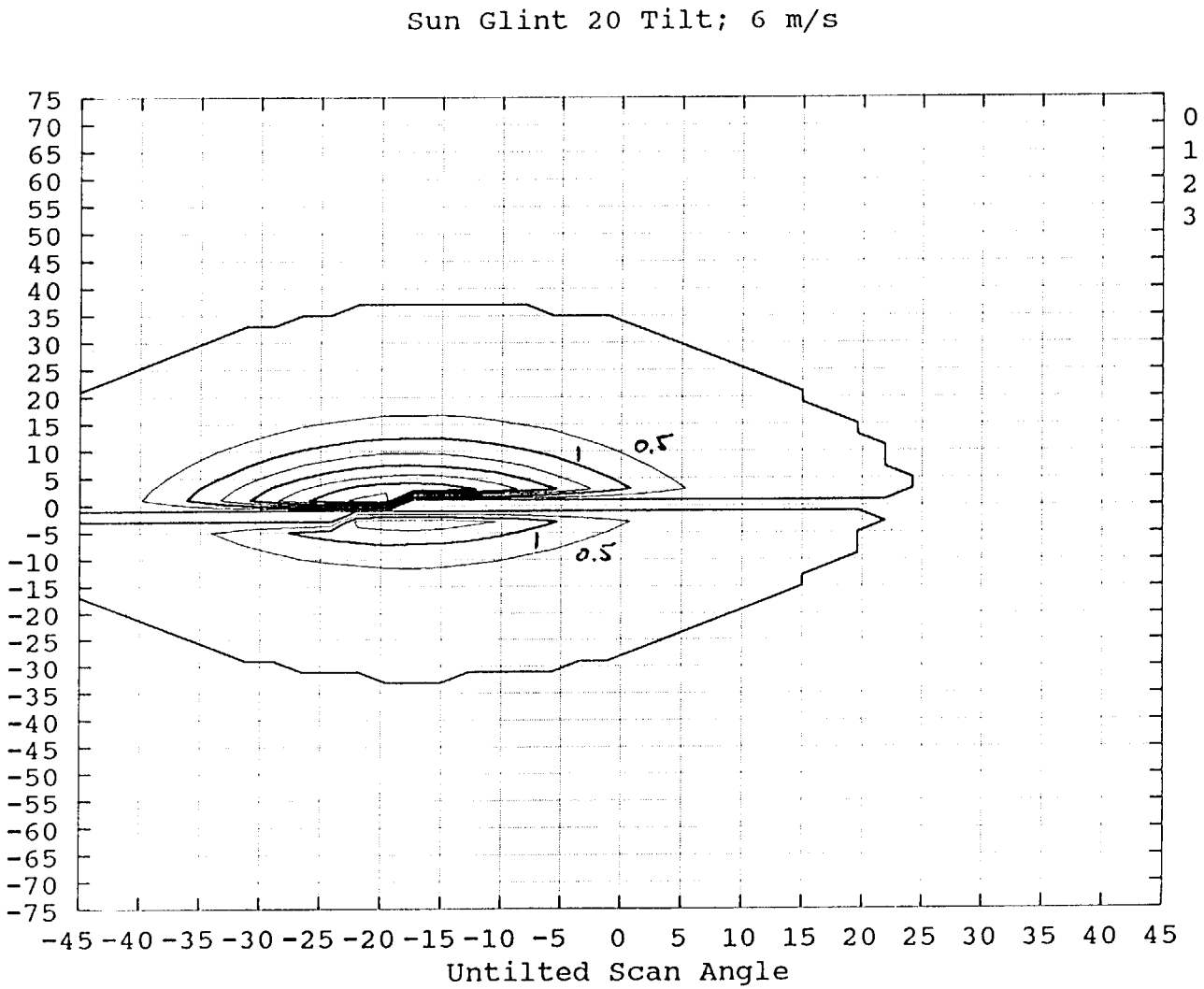

Figure 4. Sun glint radiance distribution obtained by MODIS-T for 20° tilt, with a 6 m s^{-1} wind speed. Latitude of the pixel is on the ordinate, untilted scan angle on the abscissa. Units are mW cm^{-2} μm^{-1} sr^{-1}. The numbers on the right-hand side denote the major contour levels (in bold).

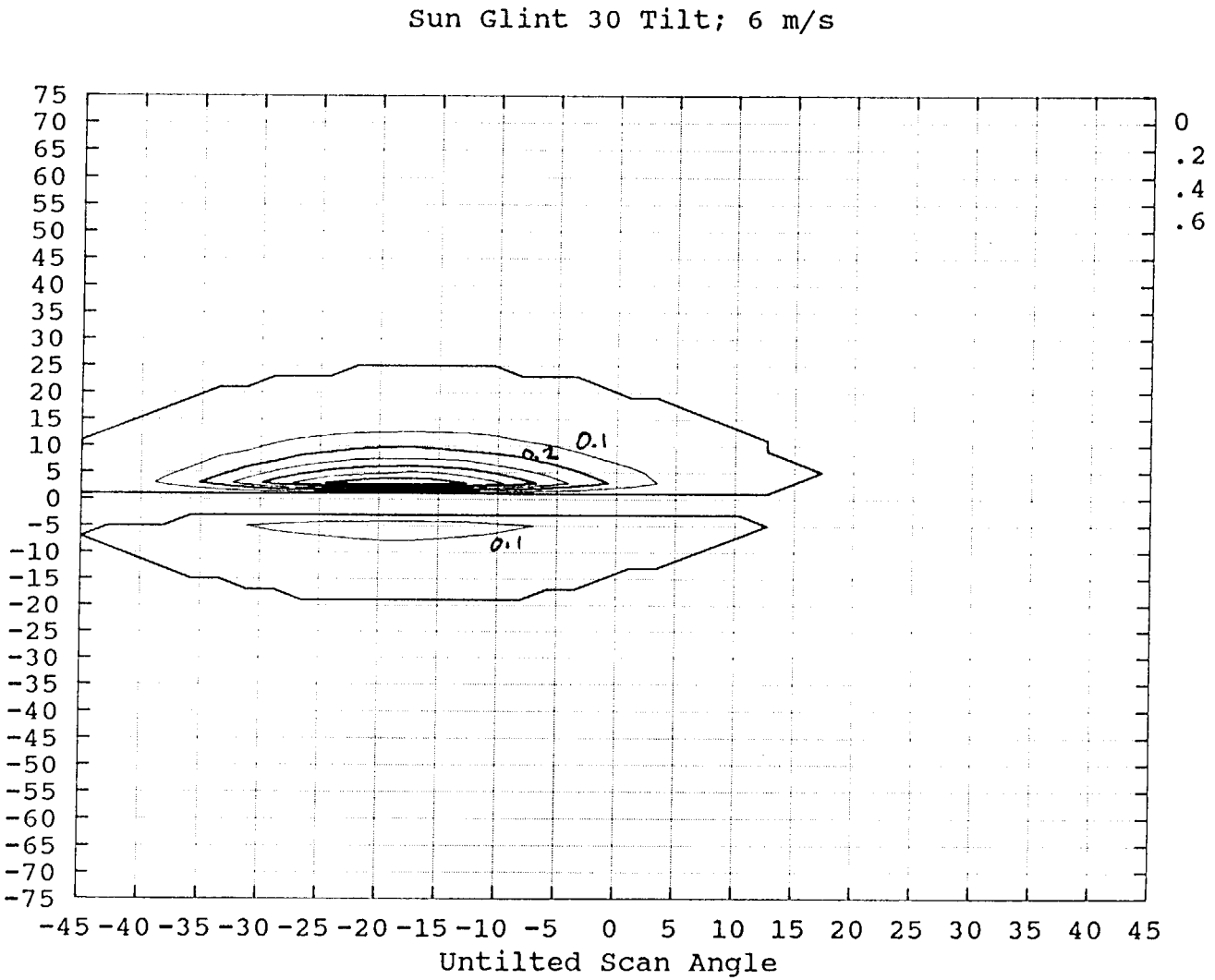

Figure 5. Sun glint radiance distribution obtained by MODIS-T for 30° tilt, with a 6 m s^{-1} wind speed. Latitude of the pixel is on the ordinate, untilted scan angle on the abscissa. Units are mW cm^{-2} μm^{-1} sr^{-1}. The numbers on the right-hand side denote the major contour levels (in bold).

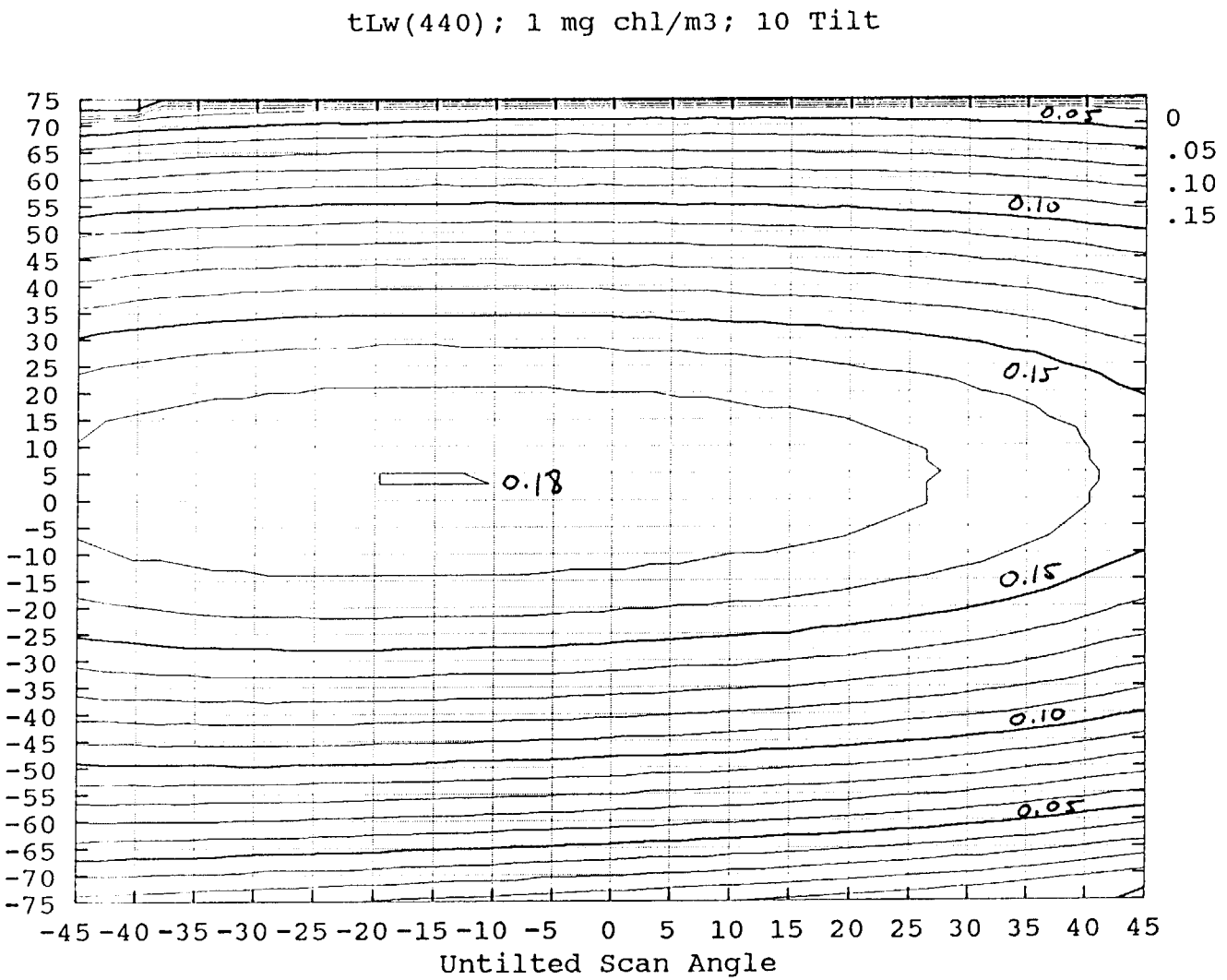

Figure 6. Distribution of diffusely transmitted water-leaving radiance (tL_w) at 440 nm obtained by MODIS-T for 10° tilt, with a 6 m s^{-1} wind speed. Latitude of the pixel is on the ordinate, untilted scan angle on the abscissa. Units are mW cm^{-2} μm^{-1} sr^{-1}. The numbers on the right-hand side denote the major contour levels (in bold).

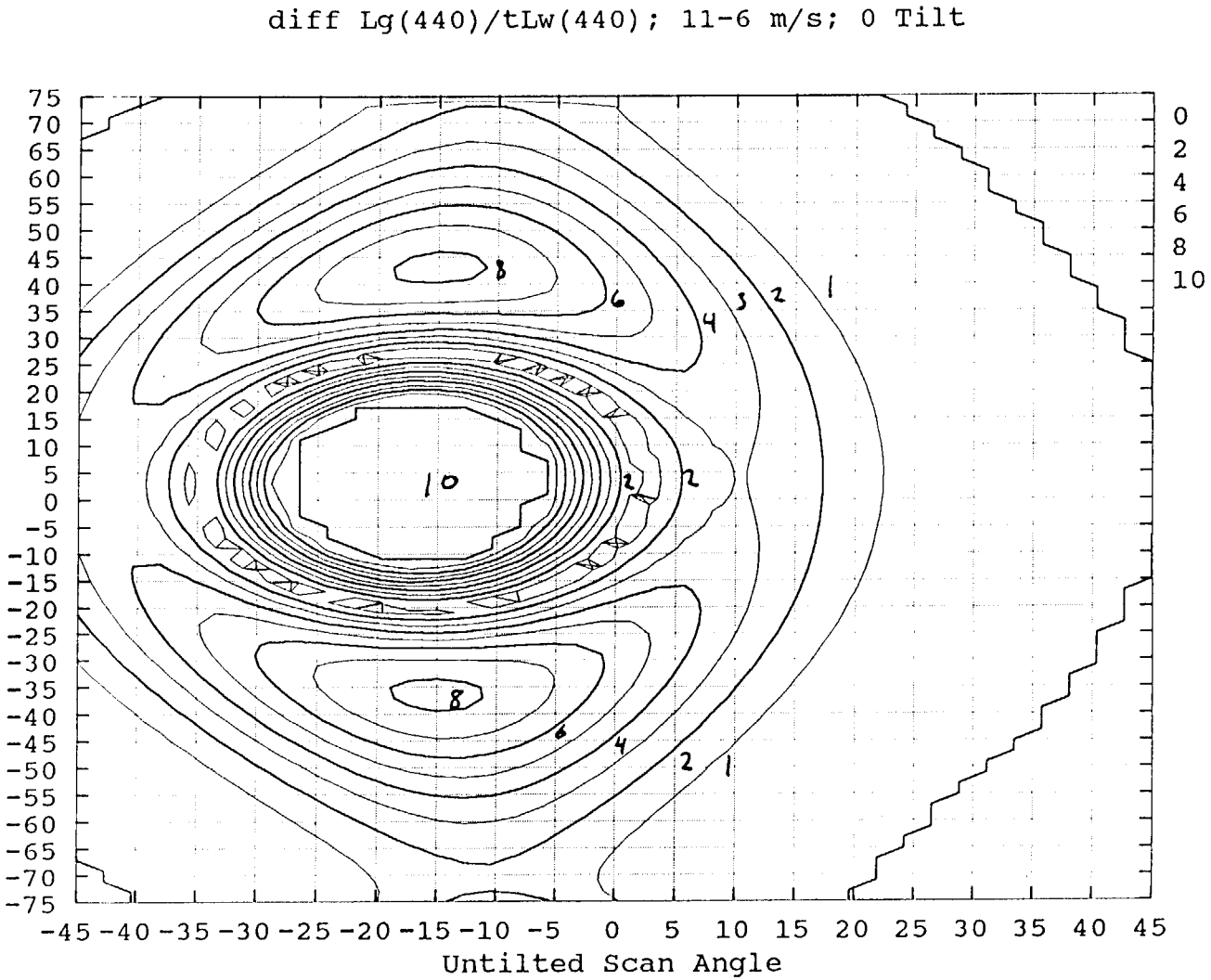

Figure 7. Distribution of the ratio $\Delta tL_g(440)$ at 11 m s^{-1} and 6 m s^{-1} to $tL_w(440)$ for a 0 tilt. Latitude of the pixel is on the ordinate, untilted scan angle on the abscissa. Units are mW cm^{-2} μm^{-1} sr^{-1}. The numbers on the right-hand side denote the major contour levels (in bold).

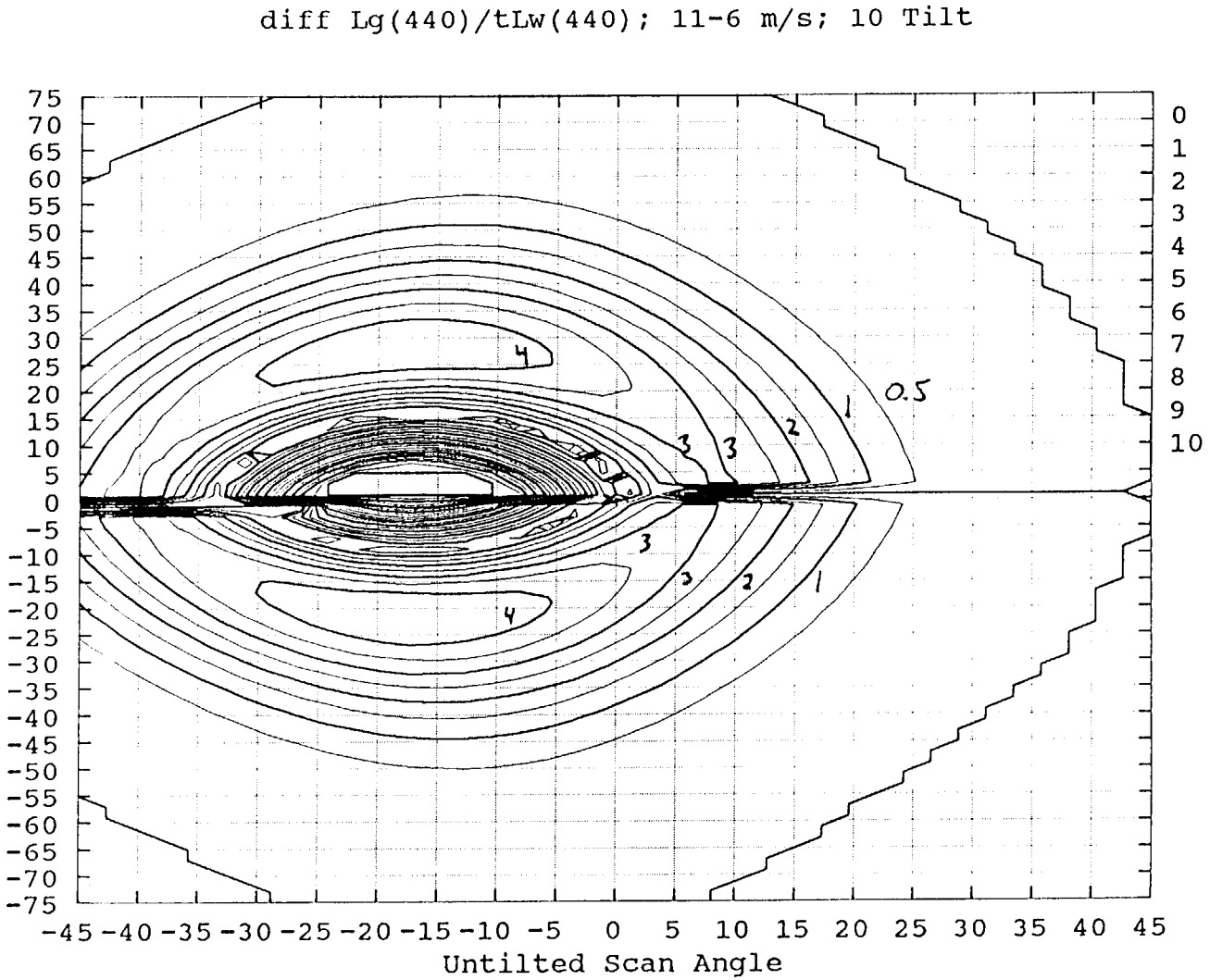

Figure 8. Distribution of the ratio $\Delta tL_g(440)$ at 11 m s^{-1} and 6 m s^{-1} to $tL_w(440)$ for a 10° tilt. Latitude of the pixel is on the ordinate, untilted scan angle on the abscissa. Units are mW cm^{-2} μm^{-1} sr^{-1}. The numbers on the right-hand side denote the major contour levels (in bold).

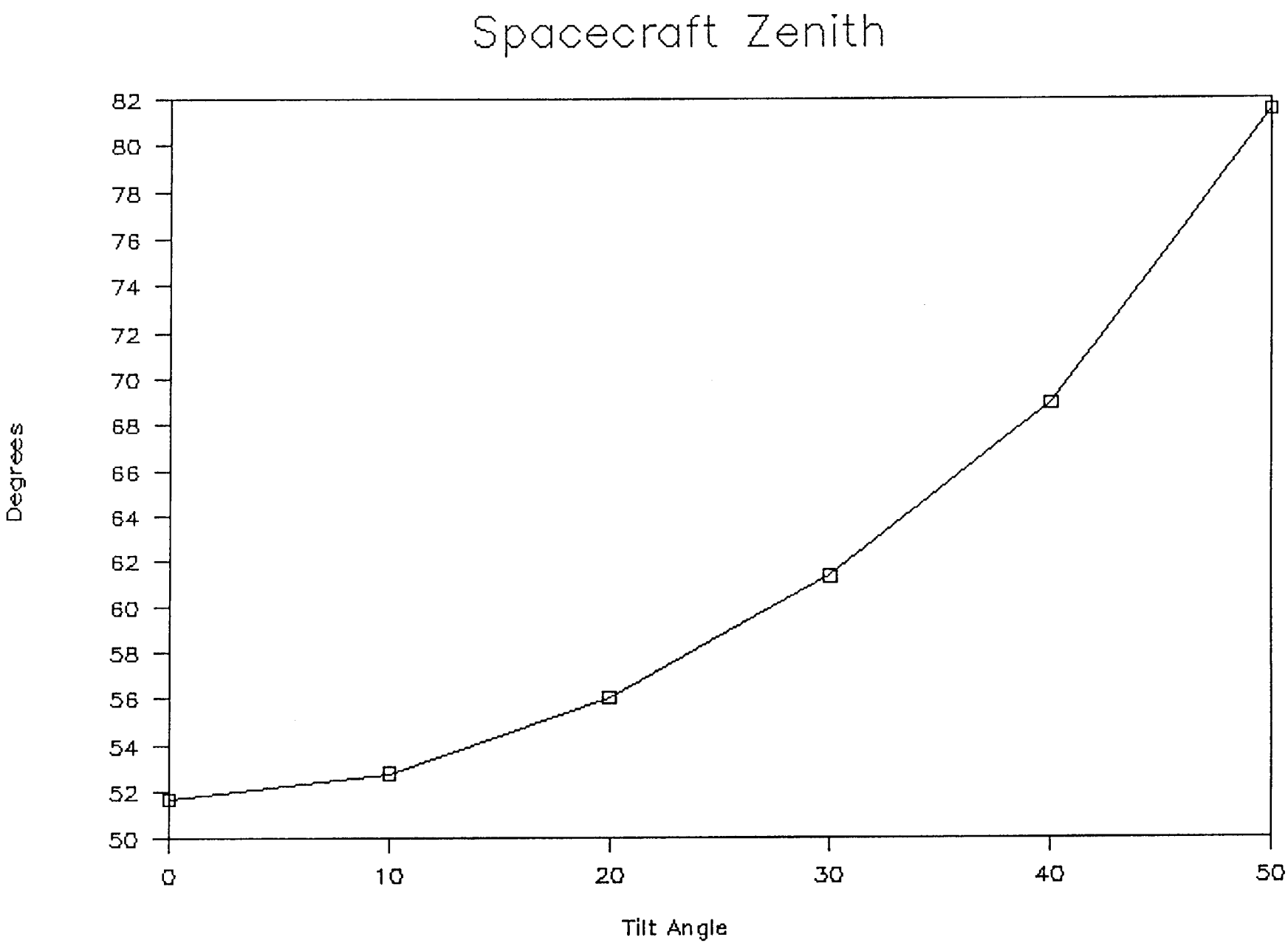

Figure 9. Maximum spacecraft zenith angle as a function of latitude and tilt.

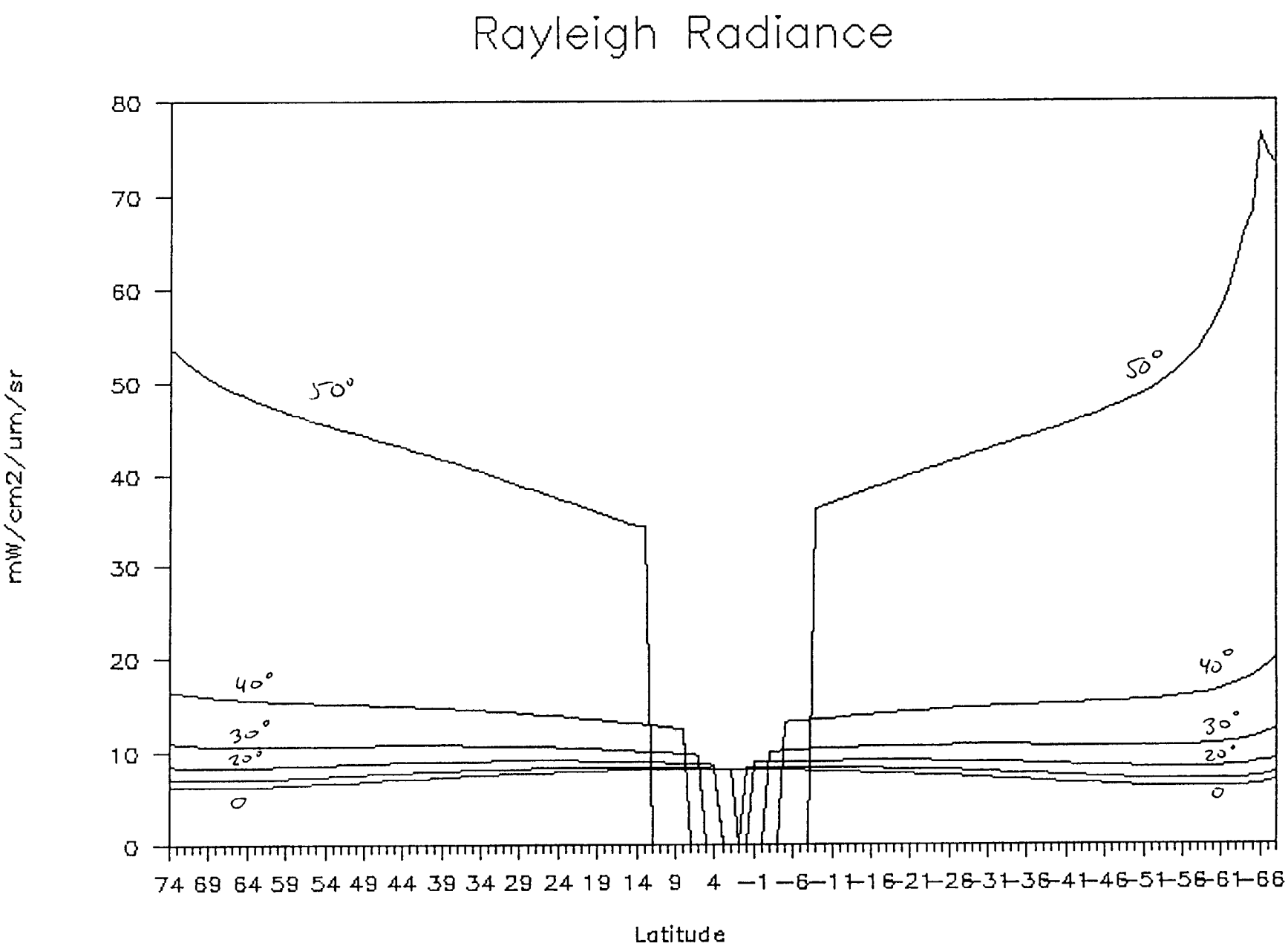

Figure 10. Single scattering Rayleigh radiance at the scan edge (right-hand or east side) as a function of latitude and tilt.

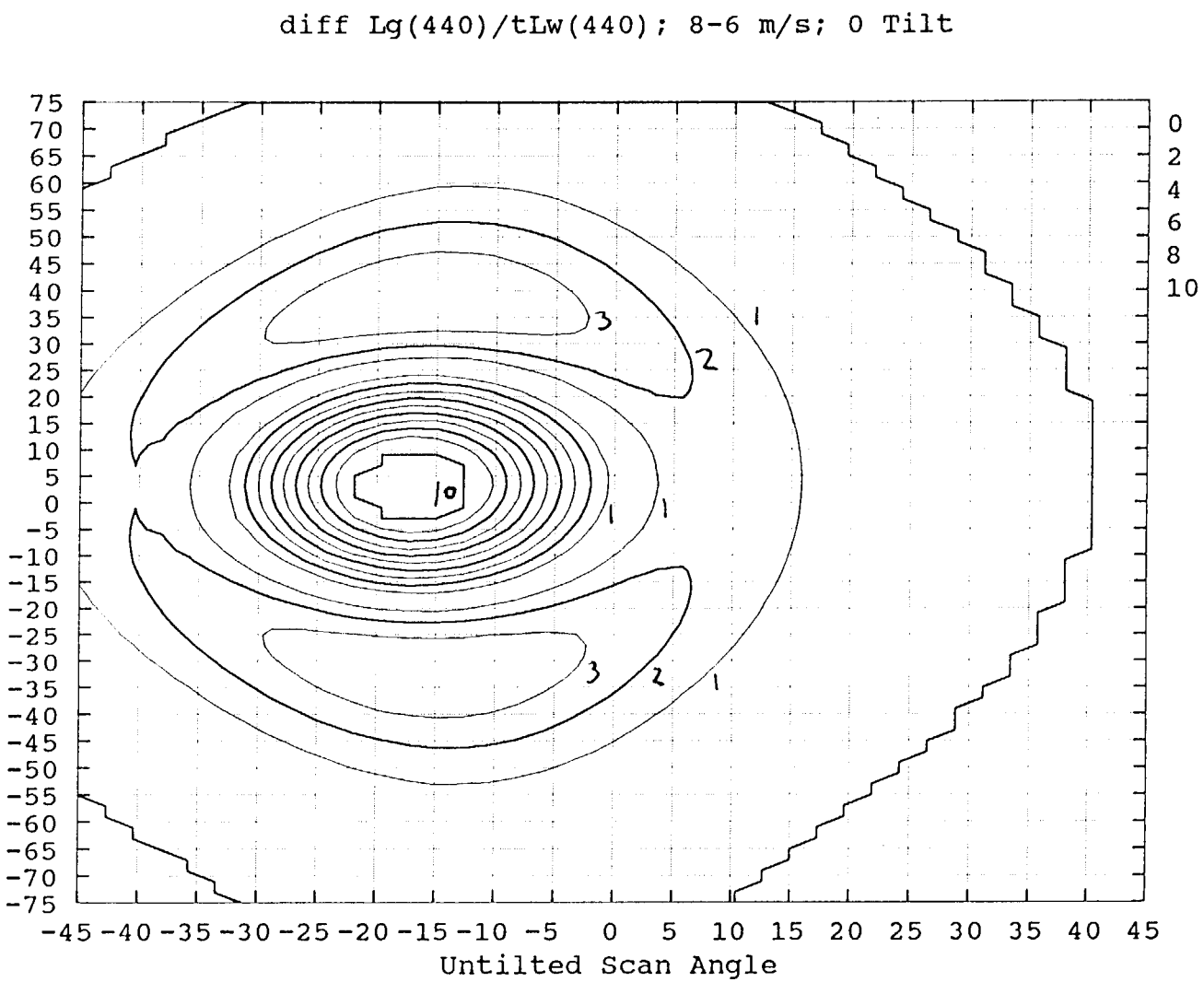

Figure 11. Distribution of the ratio $\Delta tL_g(440)$ at 8 m s^{-1} and 6 m s^{-1} to $tL_w(440)$ for a 10° tilt. Latitude of the pixel is on the ordinate, untilted scan angle on the abscissa. Units are mW cm^{-2} μm^{-1} sr^{-1}. The numbers on the right-hand side denote the major contour levels (in bold).